Orbital-Level Insights into Multifunctional Electrocatalysis of Transition-Metal Single Atoms Anchored on WS_2 Monolayers

Bingling He[1,2], Mingyang Ren[1,4], Qianyi Bu[1], Liying Zhang[2], Song Ye[1], Mengyin Liu[1], Peng Lv[5*]

Zhixue Tian[6*], Yu Jia[2,3*]

[1]*School of Electronic Engineering, Chaohu University, Hefei 238000, China*

[2]*Key Laboratory for Special Functional Materials of Ministry of Education, and School of Materials Science and Engineering, Henan University, Kaifeng, 475001, China*

[3]*International Laboratory for Quantum Functional Materials of Henan, and School of Physics and Engineering, Zhengzhou University, Zhengzhou 450001, China*

[4]*College of Physics and Electronic Information Engineering, Guilin University of Technology, Guilin, 541004, China*

[5]*Henan Key Laboratory of High Efficiency Energy Conversion Science and Technology, Henan International Joint Laboratory of New Energy Materials and Devices, School of Physics and Electronics, Henan University, Kaifeng 475004, China*

[6] *College of Physics, Hebei Key Laboratory of Photophysics Research and Application, Hebei Normal University, Shijiazhuang 050024, China*

Support Information

[*] Corresponding author. E-mail: lvpeng@henu.edu.cn (Peng Lv)

[*] Corresponding author. E-mail: zxtian@hebtu.edu.cn (Zhixue Tian)

[*] Corresponding author. E-mail: jiayu@henu.edu.cn (Yu Jia)

Note S1 Calculations of binding energy (E_b) between the TM and WS_2

The E_b was calculated to estimate the binding ability, which is defined as:

$$E_b = E(total) - E(WS_2) - E(TM)$$

Here, E(total) and E(WS_2) represent the total energies of the WS_2 monolayer with and without the anchored atoms, respectively. E(TM) is the energy of the TM atom in vacuum. The more negative E_b represents a larger binding strength.

Note S2 The hydrogen evolution reaction (HER)

The total HER can be written as, $H^+ + e^- \rightarrow 1/2H_2$.[1] This reaction occurs at the electrode, which supplies electrons and provides an intermediate adsorption site. The mechanism typically involves two steps: $* + H^+ + e^- \rightarrow *H$ (Volmer step) for the first step, then $2*H \rightarrow H_2$ (Tafel step) or $*H + H^+ + e^- \rightarrow * + H_2$ (Heyrovsky step) for the second step.

The Gibbs free energy ($\Delta G(H)$) of hydrogen atom adsorption is defined as $\Delta G(H) = \Delta E_H + \Delta E_{ZPE} - T\Delta S$, where ΔE_H is the hydrogen chemisorption energy, E_{ZPE}, and $T\Delta S$ are the zero-point energy and the entropy contribute to the $\Delta G(H)$, respectively. As it is well established that $E_{ZPE} - T\Delta S = 0.24$ eV [1], the expression for $\Delta G(H)$ can be simplified to $\Delta G(H) = \Delta E_H + 0.24$ eV, as previous studies do.[2-3] Based on Norskov's assumption, the exchange current (i_0) expressions, $i_0 = \frac{-ek_0}{1+\exp(-\Delta G(H)/k_BT)}$ and $i_0 = \frac{-ek_0}{1+\exp(\Delta G(H)/k_BT)}$, were used for $\Delta G(H) \leq 0$ and $\Delta G(H) > 0$, respectively. [1, 4]

As there is no experimental data available, the rate constant, k_0, was set to 1, as it was treated in the references.[5-7]

Note S3 The four-electron transfer pathways of the oxygen reduction reaction (ORR) and oxygen evolution reaction (OER) under acidic conditions (pH = 0).

Both associative and dissociative mechanisms[8] of ORR have been explored. Since the OER and ORR are thermodynamically and mechanistically reversible, sharing the same intermediates but proceeding in opposite directions, only the ORR reaction pathways are presented below.

Associative mechanism:

$$* + O_2 + H^+ + e^- \rightarrow *OOH, (a)$$

$$*OOH + H^+ + e^- \rightarrow *O + H_2O, (b)$$

$$*O + H^+ + e^- \rightarrow *OH, (c)$$

$$*OH + H^+ + e^- \rightarrow * + H_2O, (d)$$

Dissociative mechanism:

$$* + O_2 + H^+ + e^- \rightarrow *O + *OH, (a')$$

$$*O + *OH + H^+ + e^- \rightarrow *OH + *OH, (b')$$

$$*O + *OH + H^+ + e^- \rightarrow *O + H_2O, (b'')$$

$$*OH + *OH + H^+ + e^- \rightarrow *OH + H_2O, (c')$$

$$*O + H^+ + e^- \rightarrow *OH, (c)$$

$$*OH + H^+ + e^- \rightarrow * + H_2O, (d)$$

The adsorption free energy of the *OH ($\Delta G(OH)$), *OOH ($\Delta G(OOH)$), and *O ($\Delta G(O)$) can be evaluated by

$$\Delta G(OH) = G(*OH) + 1/2G(H_2) - G* - G(H_2O),$$

$$\Delta G(OOH) = G(*OOH) + 3/2G(H_2) - G* - 2G(H_2O),$$

$$\Delta G(O) = G(*O) + G(H_2) - G* - G(H_2O)$$

The free-energy change, ΔG, for each step of ORR with the associative mechanism was obtained by setting $\Delta G(O_2) = 4.92$ eV and $\Delta G(H_2O) = 0$ eV at 298 K as follows:

$\Delta G_a = G(*OOH) – G* – G(O_2) – 1/2G(H_2)$

$= G(*OOH) – G* – G(O_2) – 1/2G(H_2) + 2G(H_2) – 2G(H_2)$

$= G(*OOH) – G* + 3/2\ G(H_2) – G(O_2) - 2G(H_2)$

$= G(*OOH) – G* + 3/2\ G(H_2) – 2G(H_2O) – 4.92$

$= \Delta G(OOH) – 4.92$

$\Delta G_b = G(*O) + G(H_2O) – G(*OOH) – 1/2G(H_2)$

$= G(*O) + G(H_2) − G* − G(H_2O) – G(*OOH) – 3/2G(H_2) + G* + 2G(H_2O)$

$= \Delta G(O) – \Delta G(OOH)$

$\Delta G_c = G(*OH) – G(*O) – 1/2G(H_2)$

$= G(*OH) + 1/2G(H_2) − G* − G(H_2O) – G(*O) – G(H_2) + G* + G(H_2O)$

$= \Delta G(OH) – \Delta G(O)$

$\Delta G_d = G(H_2O) + G* – 1/2G(H_2) – G(*OH)$

$= – \Delta G(OH)$

Then the overpotentials for ORR (η_{ORR}, V) can be calculated by the following equation[9]:

$\eta_{ORR} = 1.23\ V + \max (\Delta G_a, \Delta G_b, \Delta G_c, \Delta G_d)/e$

The overpotentials for OER (η_{OER}, V) are defined by[10-11]:

$\eta_{OER} = \max (–\Delta G_a, –\Delta G_b, –\Delta G_c, –\Delta G_d)/e – 1.23\ V$

Note S4 Calculation of the volcano peak for ORR and OER[12]

As shown in Figs. 4a and 4b, strong linear scaling relationships were observed between the adsorption free energies of *O (ΔG(O)) and *OOH (ΔG(OOH)) with respect to *OH (ΔG(OH)), with correlation coefficients (R^2) of 0.97 for ΔG(OOH) vs. ΔG(OH) and 0.90 for ΔG(O) vs. ΔG(OH), respectively, as follows:

$\Delta G(OOH) = 0.84\Delta G(OH) + 2.97$ ($R^2 = 0.97$)

$\Delta G(O) = 1.39\Delta G(OH) + 0.78$ ($R^2 = 0.90$)

According to Table S4, the potential-determining step (PDS) of ORR for most systems is the formation of the second H_2O molecule, except for Pd@WS_2, where the formation of *OOH is the PDS.

When the formation of the second H_2O molecule is the PDS, the overpotential for the ORR can be calculated as:

$\eta_{ORR} = \Delta G_d/e + 1.23$ V

$= -\Delta G(OH)/e + 1.23$ V

When the formation of *OOH is the PDS, the ORR overpotential is:

$\eta_{ORR} = \Delta G_a/e + 1.23$ V

$= (\Delta G(OOH) - 4.92)/e + 1.23$ V

At the volcano peak, these two expressions yield the same η_{ORR}, from which the optimal ΔG(OH) and corresponding η_{ORR} at the volcano apex are determined to be 1.06 eV and 0.17 V, respectively.

Similarly, for the OER, Table S4 shows that the PDS is typically the reaction of *O with a second H_2O molecule to generate *OOH and H^+, except for Co@WS_2 and Pd@WS_2. For Co@WS_2, the PDS is the formation of O_2, but the energy difference between O_2 formation and *OOH formation is within 0.1 eV, so the *OOH formation step is reasonably treated as the PDS. For Pd@WS_2, the dissociation of *OH into *O and H^+

is the PDS.

When the formation of *OOH and H^+ is the PDS, the OER overpotential is calculated as:

$\eta_{OER} = -\Delta G_b/e - 1.23$ V

$= \Delta G(OOH) - \Delta G(O) - 1.23$ V

When the dissociation of *OH is the PDS, the OER overpotential is:

$\eta_{OER} = -\Delta G_c/e - 1.23$ V

$= \Delta G(O) - \Delta G(OH) - 1.23$ V

At the volcano peak, both expressions give the same η_{OER}, resulting in an optimal $\Delta G(OH)$ of 1.50 eV and a corresponding η_{OER} of 0.14 V.

Note S5 Calculations of formation energy (E_f) and the dissolution potential (U_{diss}) for TM@WS_2.

The thermodynamic stability and electrochemical stability were evaluated by the formation energy (E_f) and the dissolution potential (U_{diss}), defined as[13]:

$$E_f = E(total) - E(WS_2) - E(TM\text{-}bulk)$$

$$U_{diss} = U^0 - E_f/ne$$

Where E(total) and E(WS_2) are the total energies of WS_2 with and without the TM atom, respectively, and E(TM-bulk) is the energy of the TM atom in their bulk. U^0 denotes the standard dissolution potential of bulk TM, and n is the number of electrons involved in the dissolution. The values of U^0 and n comes from the previous literature.[13]

Table S1 Zero-point energy corrections and entropic contributions (at 298.15 K) to the free energies.

species	ΔE_{ZPE} (eV)	$T\Delta S$ (eV)
H_2O	0.56	0.67
H_2	0.27	0.40
*OOH	0.42	0.216
*OH	0.32	0.09
*O	0.05	0.11

Table S2 Charge transfer amounts (Q(TM), *e*) of TM atoms, the Fe-S bond length (d(Fe-S), Å) and the adsorption free energies (ΔG, eV) of the O, OH and OOH. A negative Q(TM) indicates electron transfer from the TM atom to the WS_2 substrate.

	Q(TM)	**d(Fe-S)**	**ΔG(OOH)**	**ΔG(O)**	**ΔG(OH)**	**ΔG(H)**
U=0	−0.56	2.145 / 2.145 / 2.145	2.92	0.27	-0.63	0.07
U=1	−0.56	2.153 / 2.152 / 2.152	2.83	0.25	-0.65	0.002
U=2	−0.55	2.165 / 2.163 / 2.163	2.50	0.25	-0.67	-0.07
U=3	−0.53	2.170 / 2.169 / 2.169	2.46	0.24	-0.72	-0.17
U=4	−0.52	2.174 / 2.174 / 2.174	2.39	0.20	-0.80	-0.30

Table S3 Binding energies (E_b, eV) of TM atoms at the S-top (E_b(S)), hollow (E_b(H)), and W-top sites (E_b(T)) on WS_2, formation energy (E_f, eV), and dissolution potential (U_{diss}, V) of TM@WS_2. Also listed are the *d*-band centers (ε_d, eV) and charge transfer amounts (Q(TM), *e*) of TM atoms. A negative Q(TM) indicates electron transfer from the TM atom to the WS_2 substrate.

	E_b(S)	E_b(H)	E_b(T)	E_f	U_{diss}	ε_d	Q(TM)
Fe	−0.92	−2.07	−2.44	3.01	−1.96	−1.13	−0.56
Co	−1.49	−2.51	−3.00	2.64	−1.60	−1.13	−0.43
Ni	−2.30	−3.39	−3.91	1.67	−1.10	−1.04	−0.36
Ru	−2.07	−2.52	−3.47	4.10	−1.59	−1.54	−0.31
Rh	−2.41	−2.68	−3.49	3.09	−0.94	−1.63	−0.18
Pd	−2.00	−2.09	−2.45	1.87	0.01	−1.70	−0.15
Os	−1.81	−2.18	−3.13	5.91	0.10	−1.64	−0.30
Ir	−2.48	−3.00	−3.44	4.52	−0.35	−1.99	−0.11
Pt	−2.88	−2.59	−3.23	3.10	−0.37	−2.26	−0.024

Table S4 H adsorption free energy (ΔG(H), eV), electron transfer to the adsorbed H atom (ΔQ(H), *e*), integrated crystal orbital Hamilton population between TM and H (ICOHP(TM–H)), adsorption free energy of the second H atom (ΔG_{sec}(H), eV), and energy barrier for H_2 formation (ΔE_{H2}, eV) on TM@WS_2.

	ΔG(H)	**Q(H)**	**ICOHP(TM-H)**	**ΔG_{Sec}(H)**	**ΔE_{H2}**
Fe	0.07	0.39	−2.10	−0.21	0.59
Co	0.11	0.14	−2.29	−0.52	0.81
Ni	0.68	0.23	−1.96	---	
Ru	−0.19	0.16	−2.58	−0.08	0.68
Rh	−0.27	0.07	−2.65	---	
Pd	0.83	0.13	−2.26	---	
Os	−0.64	0.21	−2.84	---	
Ir	−0.76	0.11	−2.93	---	
Pt	−0.01	0.08	−2.47	−0.87	1.29

Table S5 The potential-determining steps (PDS) for the ORR and OER on TM@WS_2.

	PDS (ORR)	**PDS (OER)**
Fe	$*OH+H_2O+H^++e^-\rightarrow 2H_2O$	$*O+H_2O+2H^++2e^-\rightarrow *OOH+3H^++3e^-$
Co	$*OH+H_2O+H^++e^-\rightarrow 2H_2O$	$*OOH+3H^++3e^-\rightarrow O_2+4H^++4e^-$
Ni	$*OH+H_2O+H^++e^-\rightarrow 2H_2O$	$*O+H_2O+2H^++2e^-\rightarrow *OOH+3H^++3e^-$
Ru	$*OH+H_2O+H^++e^-\rightarrow 2H_2O$	$*O+H_2O+2H^++2e^-\rightarrow *OOH+3H^++3e^-$
Rh	$*OH+H_2O+H^++e^-\rightarrow 2H_2O$	$*O+H_2O+2H^++2e^-\rightarrow *OOH+3H^++3e^-$
Pd	$O_2+4H^++4e^-\rightarrow *OOH+3H^++3e^-$	$*OH+H_2O+H^++e^-\rightarrow *O+H_2O+3H^++3e^-$
Ir	$*OH+H_2O+H^++e^-\rightarrow 2H_2O$	$*O+H_2O+2H^++2e^-\rightarrow *OOH+3H^++3e^-$
Pt	$*OH+H_2O+H^++e^-\rightarrow 2H_2O$	$*O+H_2O+2H^++2e^-\rightarrow *OOH+3H^++3e^-$

Table S6 Adsorption free energies of *OOH (ΔG(OOH), eV), *O (ΔG(O), eV), and *OH (ΔG(OH), eV), along with the calculated overpotentials for ORR (η_{ORR}, V) and OER (η_{OER}, V). Also listed are the magnetic moment on the TM site upon *OH adsorption (M_B, μ_B) and the amount of charge transferred to the *OH species (ΔQ(OH), *e*).

	ΔG(OOH)	**ΔG(O)**	**ΔG(OH)**	$\boldsymbol{\eta_{ORR}}$	$\boldsymbol{\eta_{OER}}$	$\mathbf{M_B}$	**Q(OH)**
Fe	2.92	0.27	−0.63	1.86	1.33	2.39	0.51
Co	2.77	0.60	−0.22	1.45	0.92	1.55	0.44
Ni	3.50	1.88	0.58	0.65	0.32	0.64	0.44
Ru	2.75	0.10	−0.21	1.44	1.34	1.54	0.45
Rh	3.29	1.17	0.62	0.61	0.8	1.04	0.43
Pd	4.13	2.80	1.32	0.44	0.33	0.41	0.39
Os	---	−1.24	−0.62	1.85	4.15	0.45	
Ir	2.76	0.31	−0.20	1.43	1.14	0.96	0.40
Pt	3.57	1.67	0.60	0.63	0.58	0.41	0.36

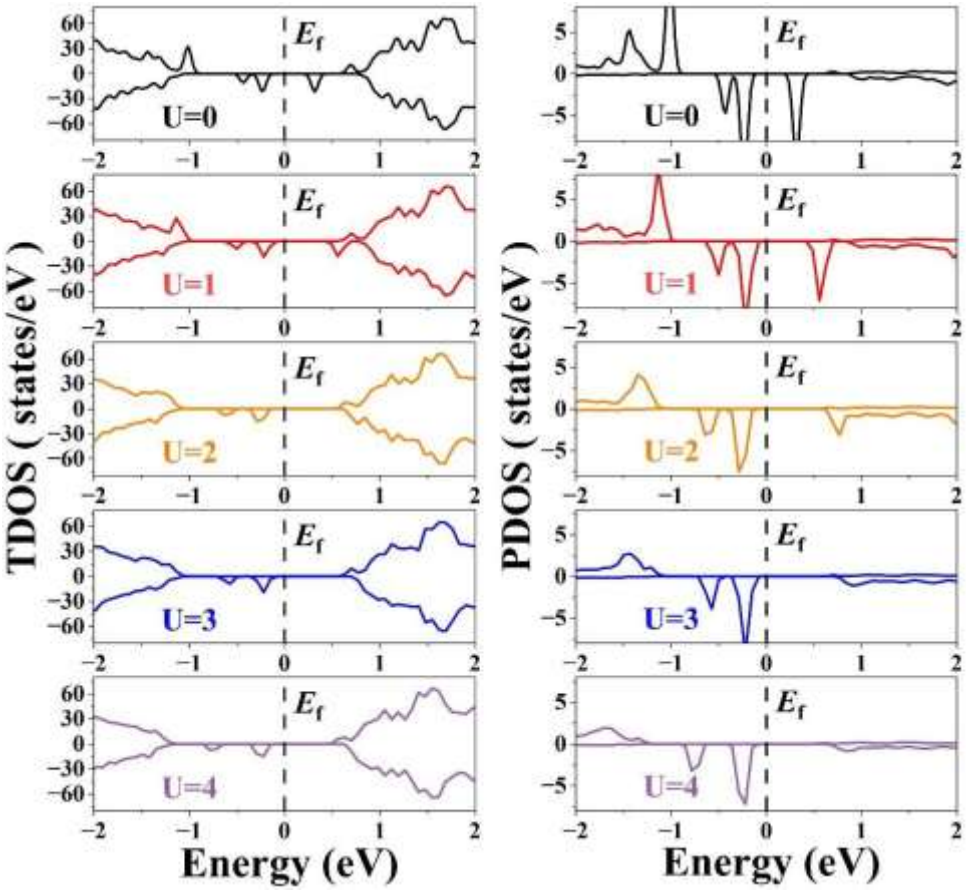

Fig. S1 Total DOS (left) and Fe-3*d* PDOS (right) of the Fe@WS_2 system.

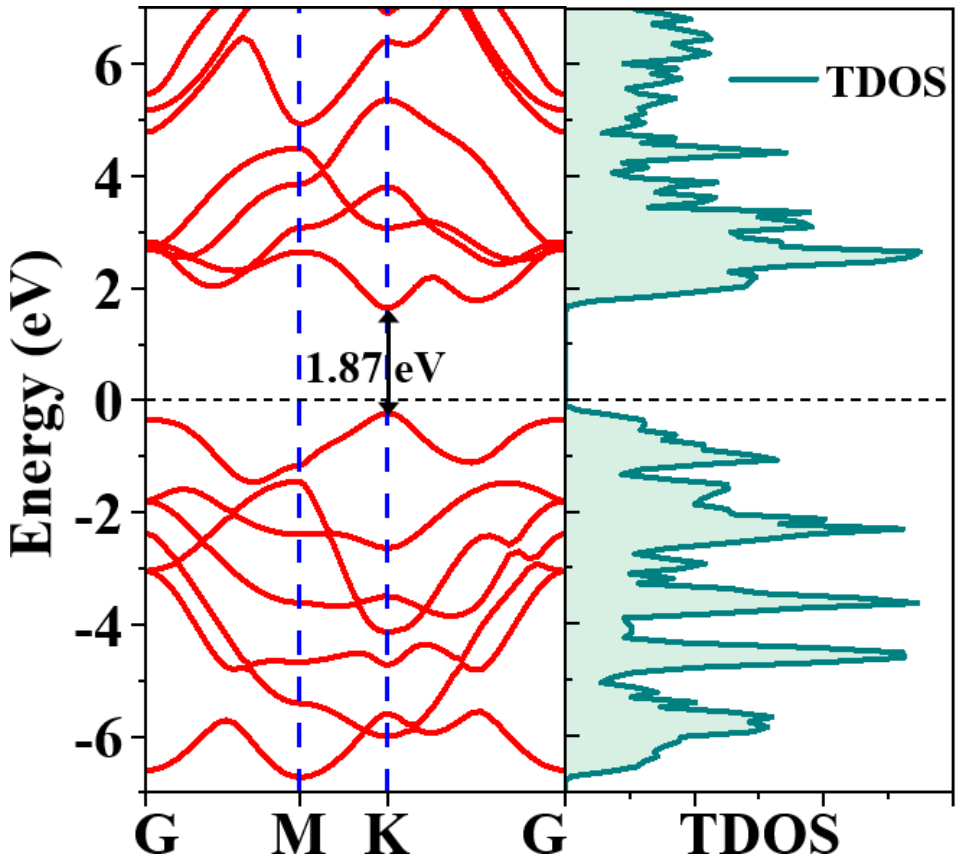

Fig. S2 Calculated band structure and total density of states (TDOS) of pristine WS_2.

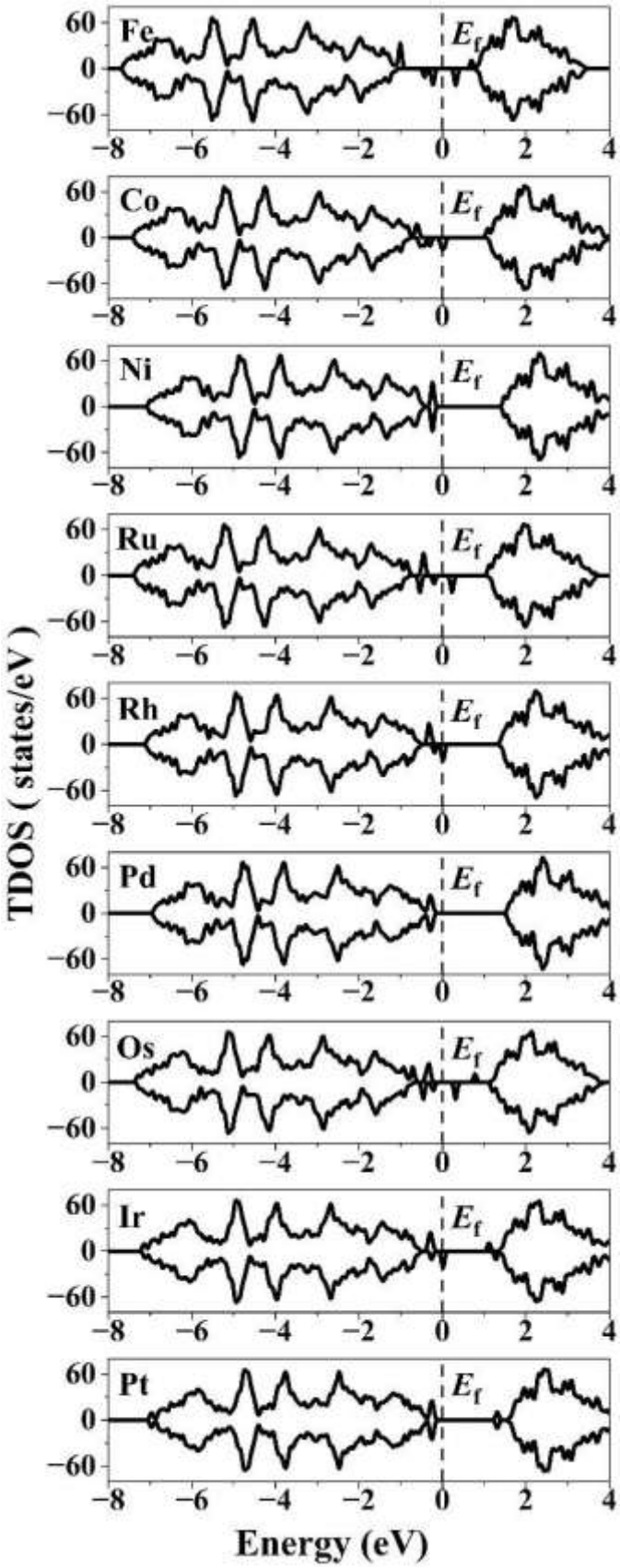

Fig. S3 Total density of states (TDOS) of TM@WS_2 systems.

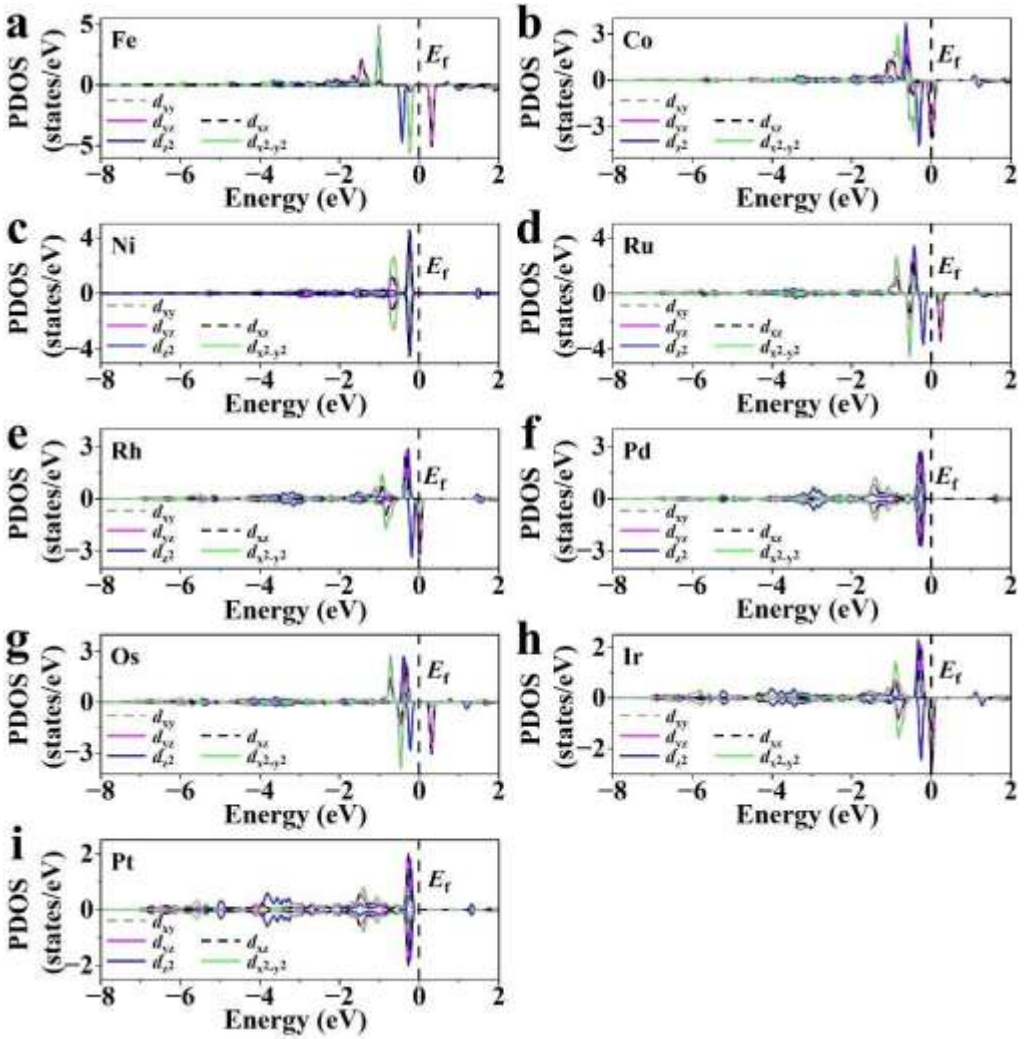

Fig. S4 Projected density of states (PDOS) of TM@WS_2 systems: (a) Fe, (b) Co, (c) Ni, (d) Ru, (e) Rh, (f) Pd, (g) Os, (h) Ir, and (i) Pt.

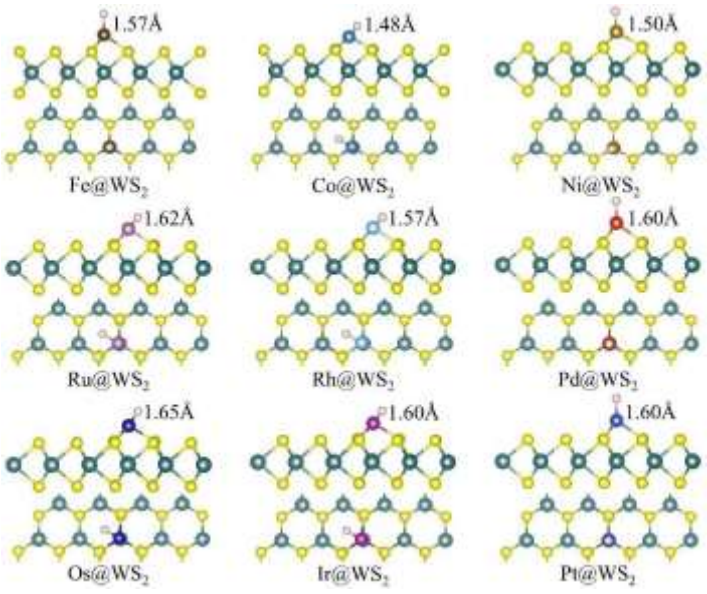

Fig. S5 Optimized atomic structures of H adsorption on TM@WS_2 with key structural parameters labeled (in Å).

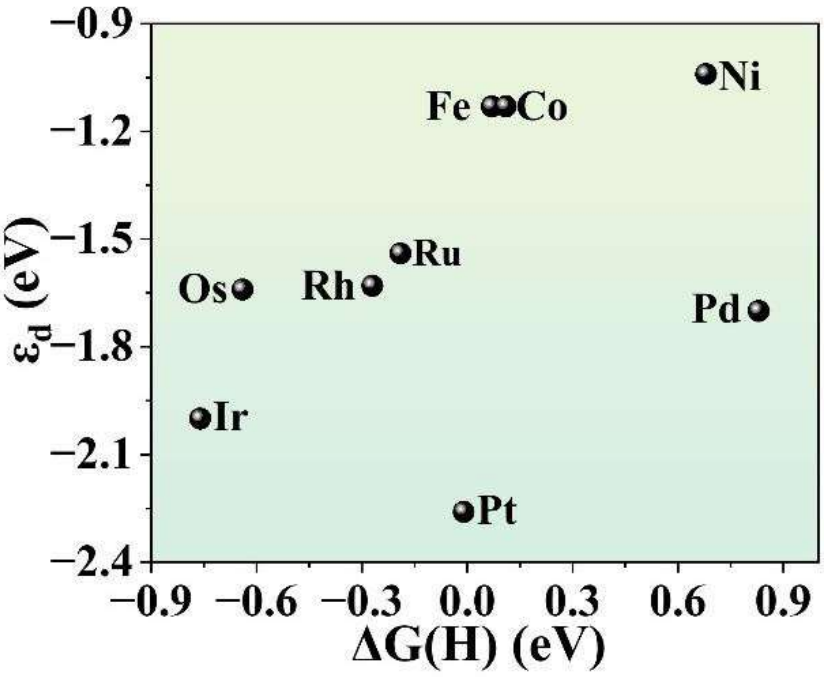

Fig. S6 Correlation between the *d*-band center (ε_d) of TM atoms and the hydrogen adsorption free energy ($\Delta G(H)$) on TM@WS_2.

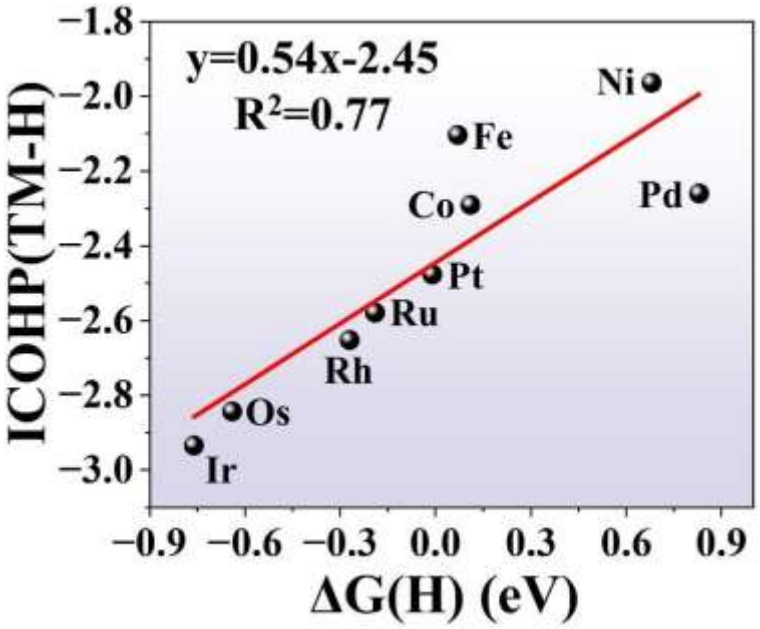

Fig. S7 Correlation between the integrated crystal orbital Hamilton population of the TM–H bond and the hydrogen adsorption free energy (ΔG(H)) on TM@WS_2.

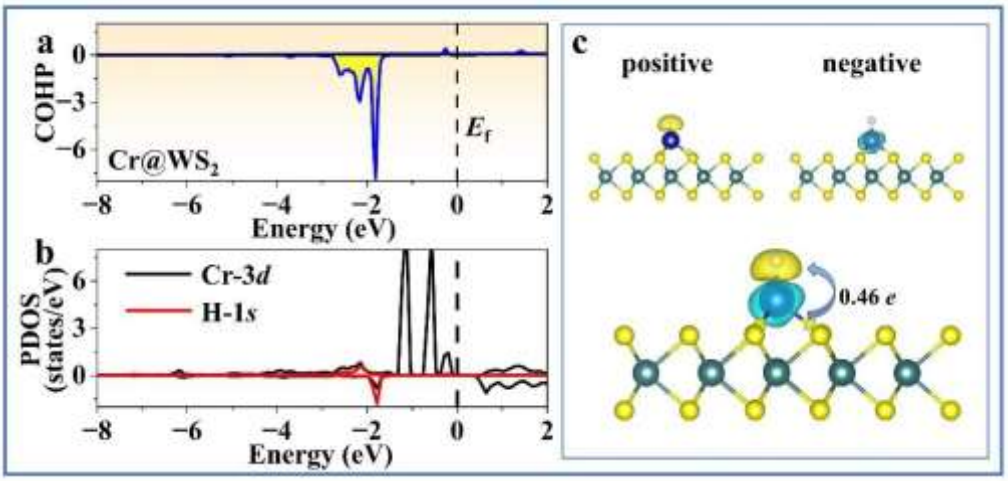

Fig. S8 (a) COHP analysis of the Cr–H interaction, (b) projected density of states (PDOS) of Cr-3*d* and H-1*s*, and (c) charge density difference (CDD) for Cr@WS_2. The isosurface value is set to 0.005 e $bohr^{-3}$ for CDD.

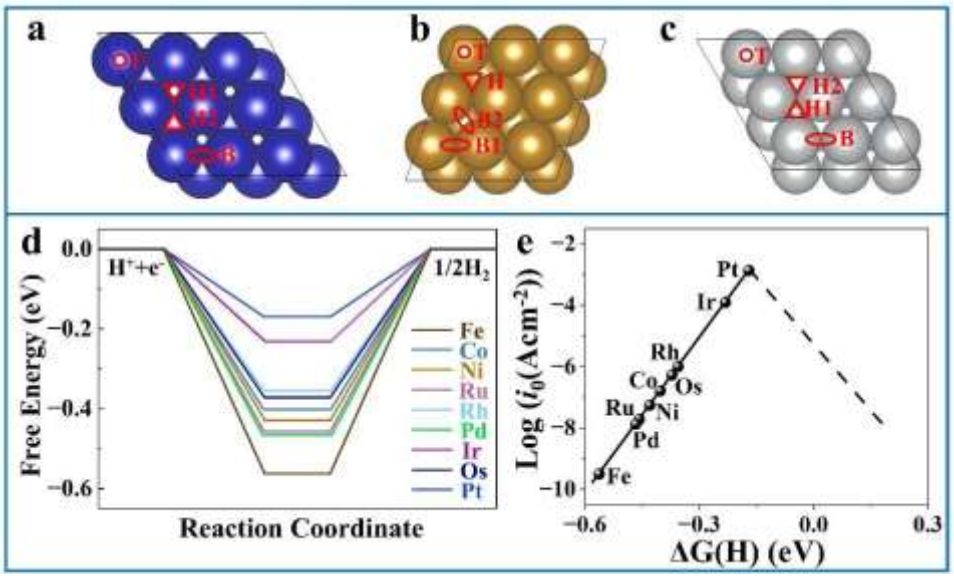

Fig. S9 (a–c) Schematic illustration of the top two atomic layers and representative adsorption sites on (a) hcp (0001), (b) bcc (110), and (c) fcc (111) metal surfaces. (d) Free energy diagrams of the HER on TM@WS_2 systems. (e) Volcano plot of the exchange current density (i_0) as a function of the hydrogen adsorption free energy ($\Delta G(H)$).

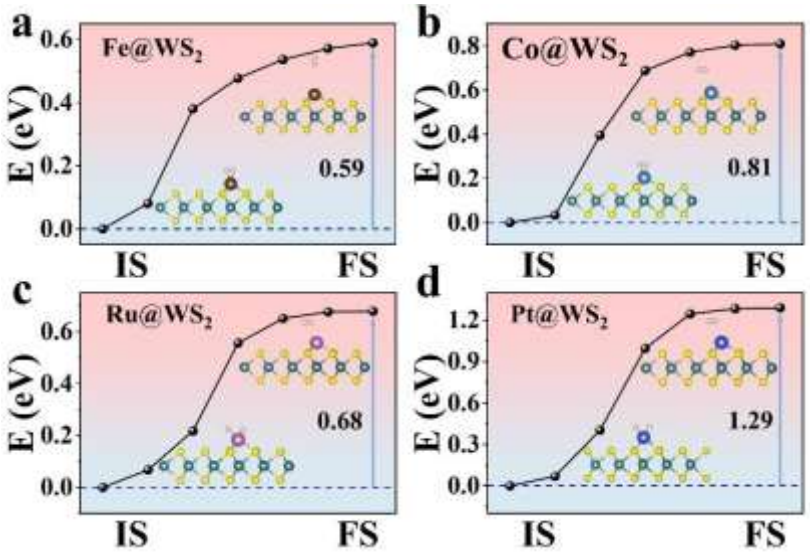

Fig. S10 Energy barriers for the formation of physisorbed H_2 via the Tafel mechanism from two adsorbed hydrogen atoms on (a) $Fe@WS_2$, (b) $Co@WS_2$, (c) $Ru@WS_2$, and (d) $Pt@WS_2$.

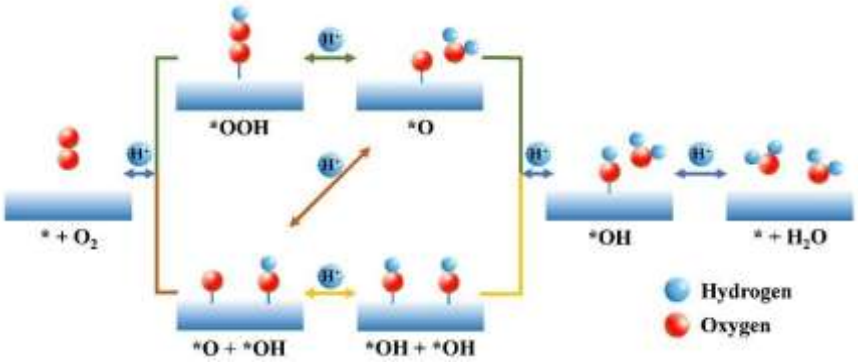

Fig. S11 Schematic illustration of the possible reaction pathways for the ORR and OER on TM@WS_2 catalysts.

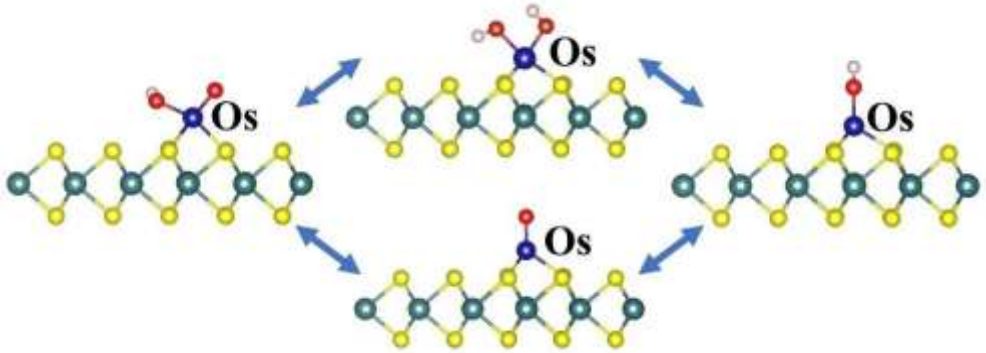

Fig. S12 The ORR and OER pathways on Os@WS_2.

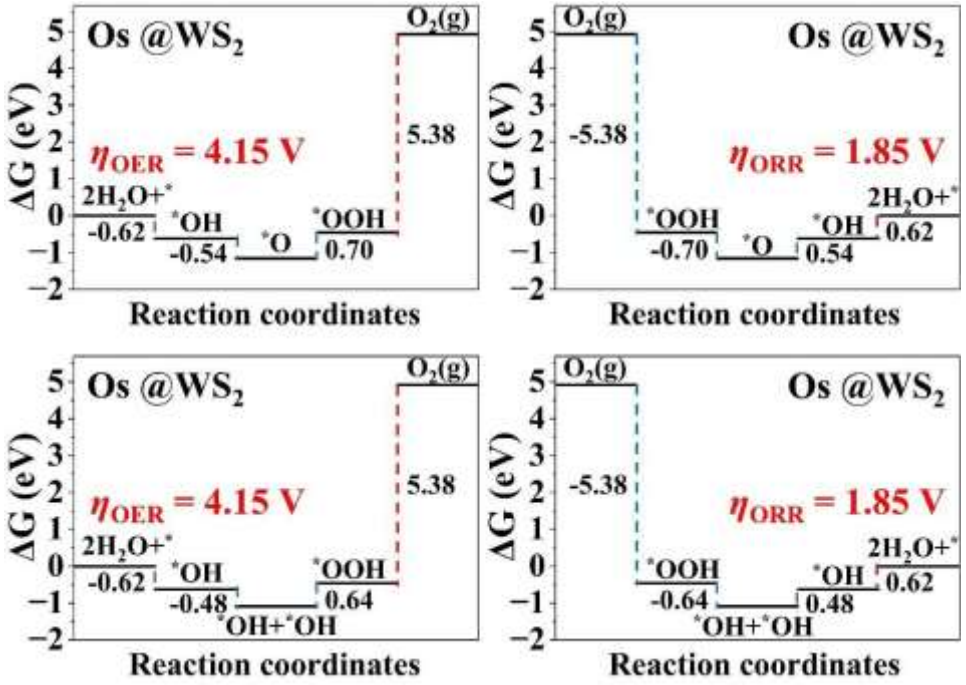

Fig. S13 Gibbs free energy change (ΔG) for each elementary step involved in the OER and ORR on Os@WS_2.

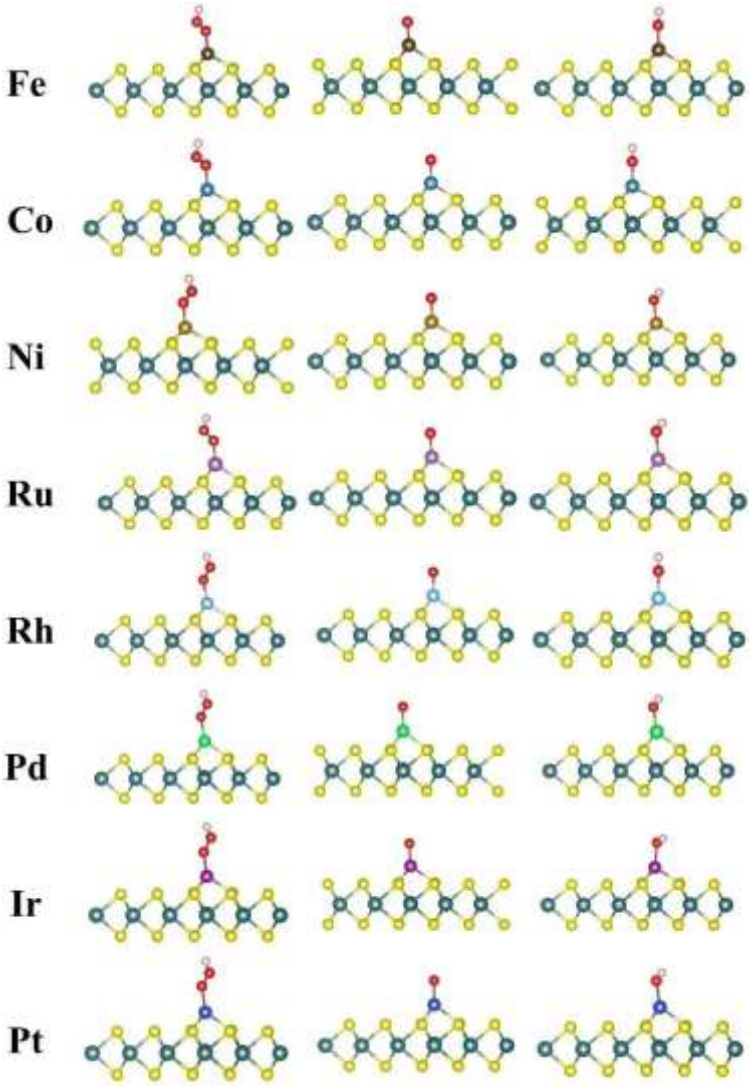

Fig. S14 Optimized atomic structures of *O, *OH, and *OOH adsorbed on TM@WS_2.

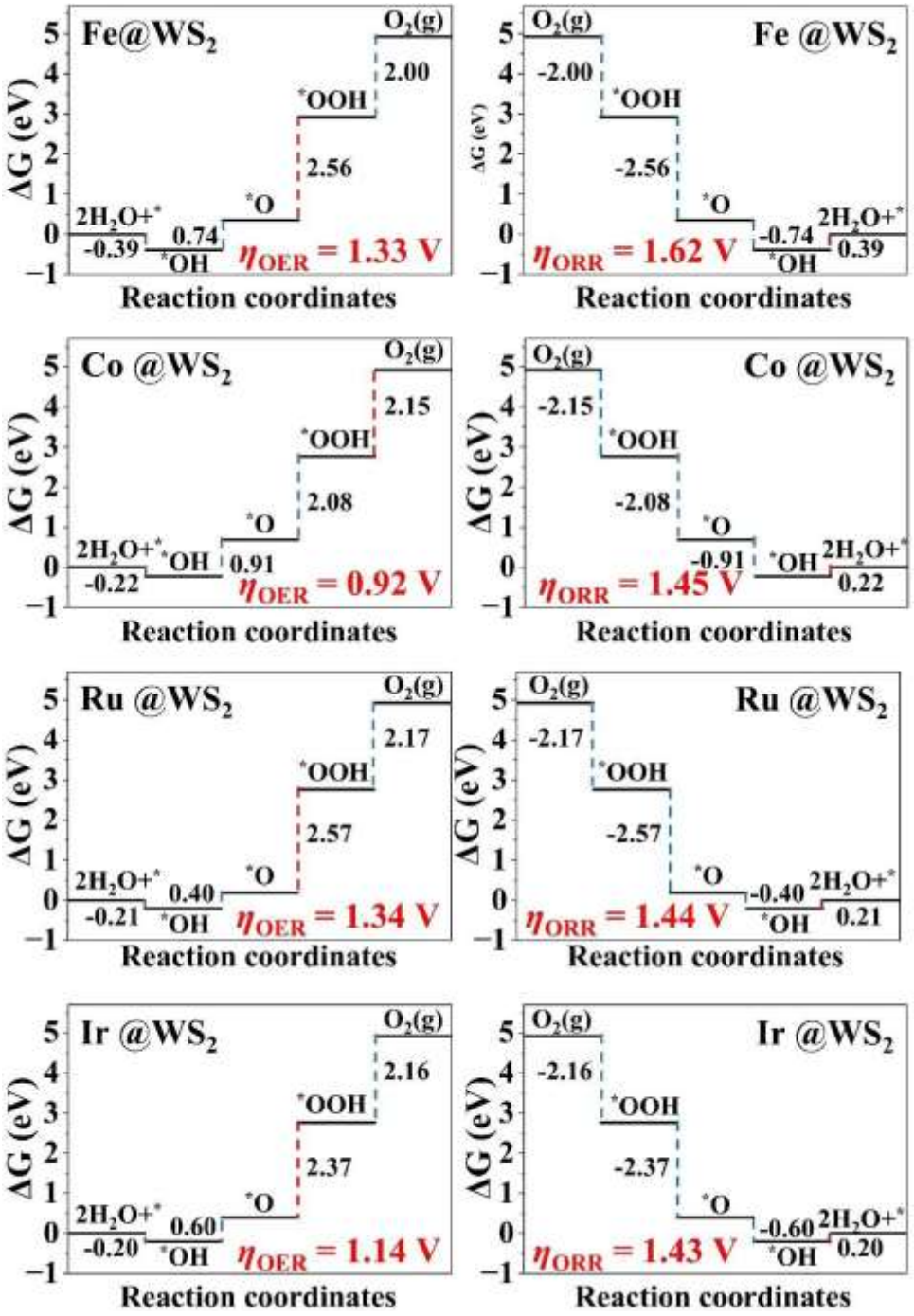

Fig. S15 Gibbs free energy change (ΔG) for each elementary step involved in the OER and ORR on Fe@WS_2, Co@WS_2, Ru@WS_2, Ir@WS_2.

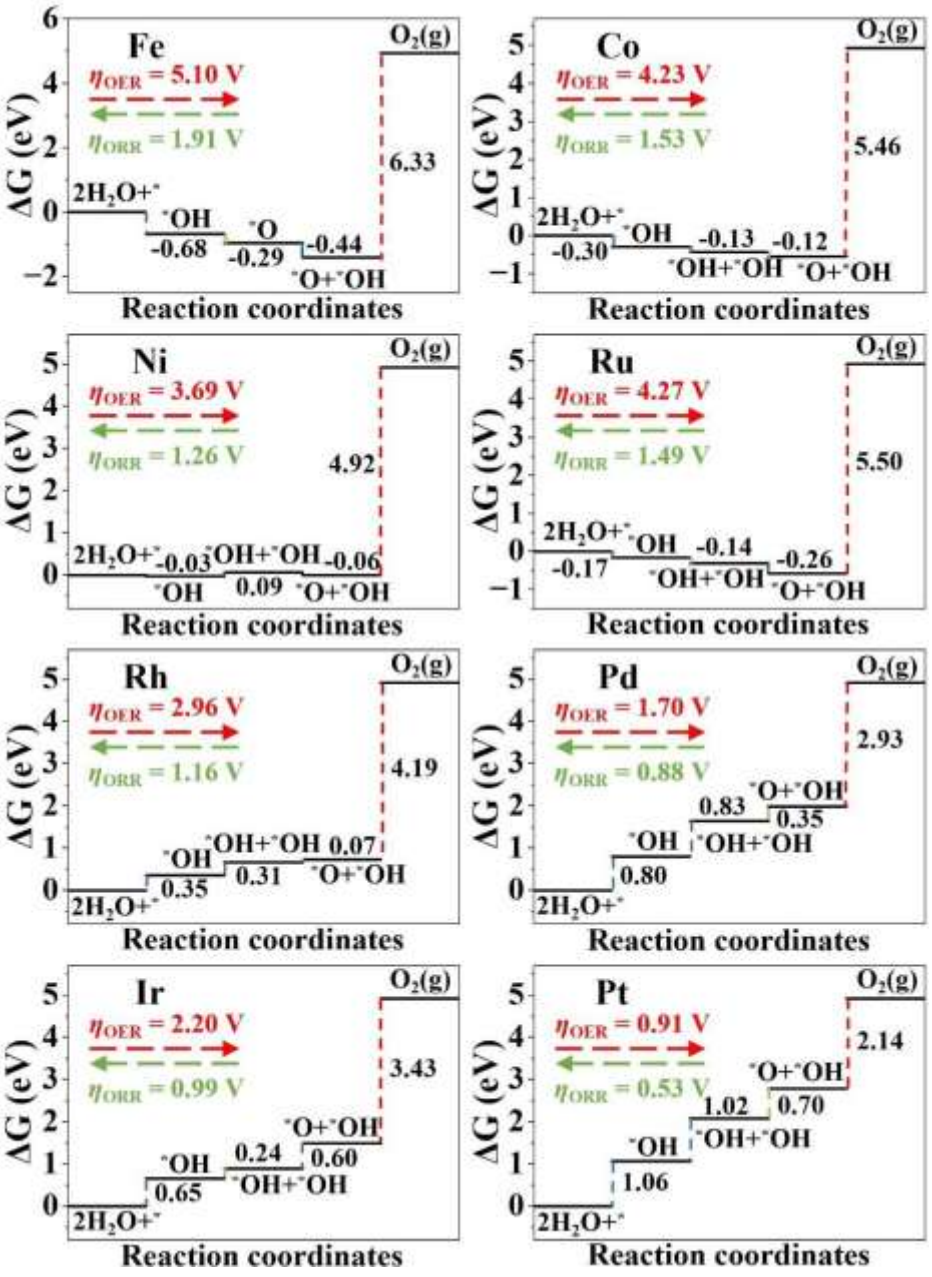

Fig. S16 Gibbs free energy changes (ΔG) for each elementary step involved in the OER and ORR on the bcc Fe (110) surface, fcc Ni, Pt, Pd, Ir, and Rh (111) surfaces, and hcp Ru, Os, and Co (0001) surfaces. Note that although the associative mechanism of ORR may also occur on bulk Pt, Ir, Pd, and Rh, its catalytic performance is inferior to that of the dissociative mechanism; thus, it is not further discussed here.

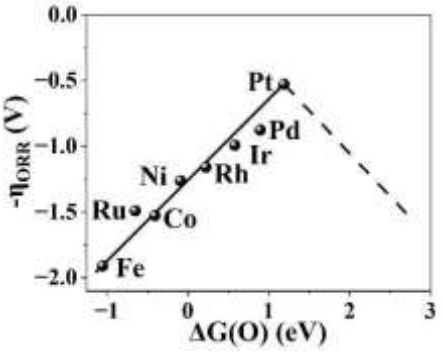

Fig. S17 Relationship between the ORR overpotential (η_{ORR}) and ΔG(O).

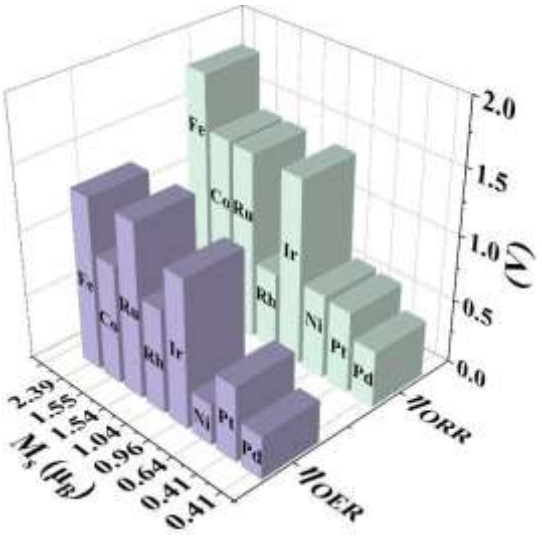

Fig. S18 Correlation between the magnetic moment on the TM site upon *OH adsorption (M_B, μ_B) and the overpotentials for OER and ORR on TM@WS_2.

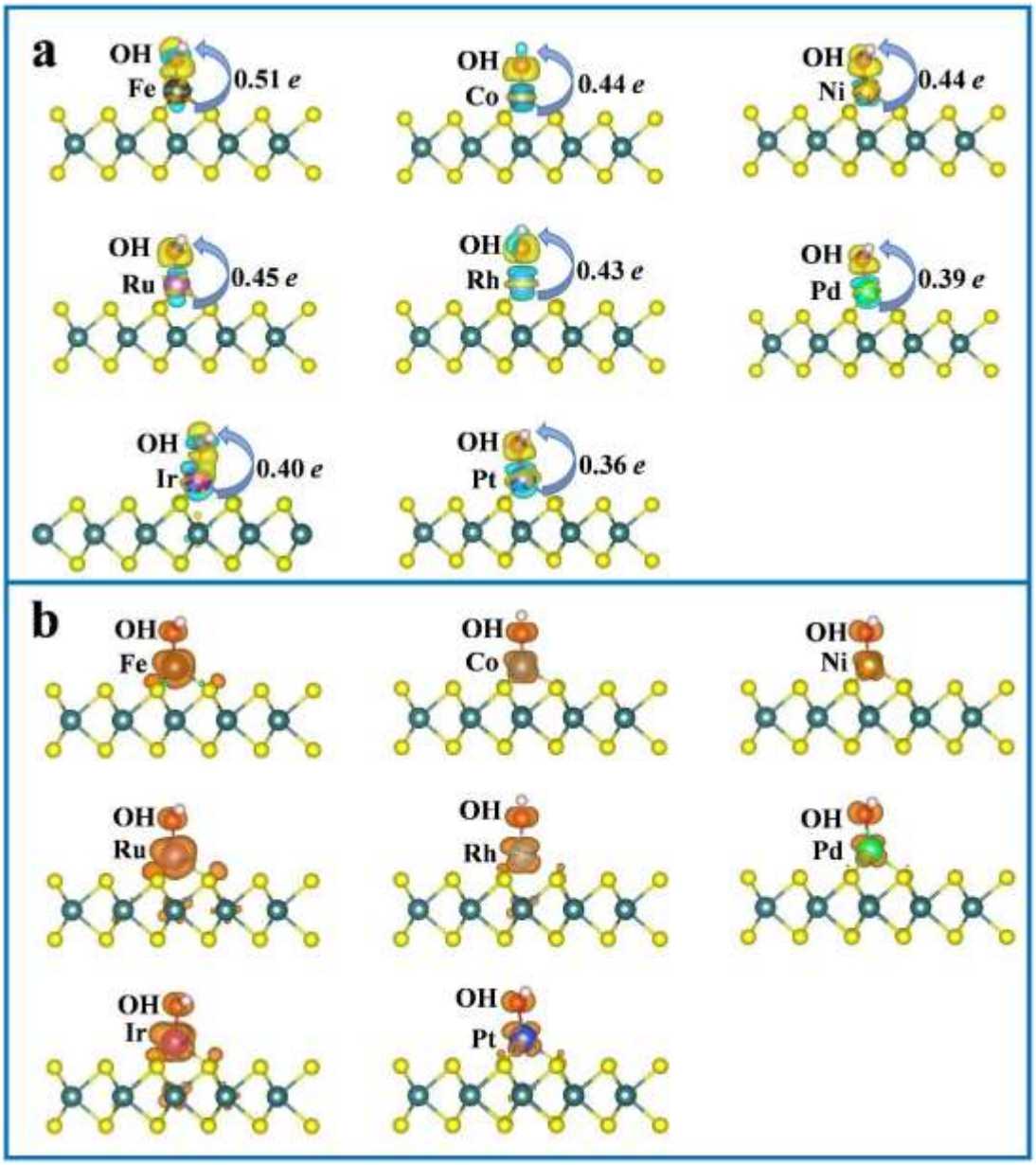

Fig. S19 (a) Charge density difference and (b) spin density distribution of TM@WS_2 with adsorbed *OH.

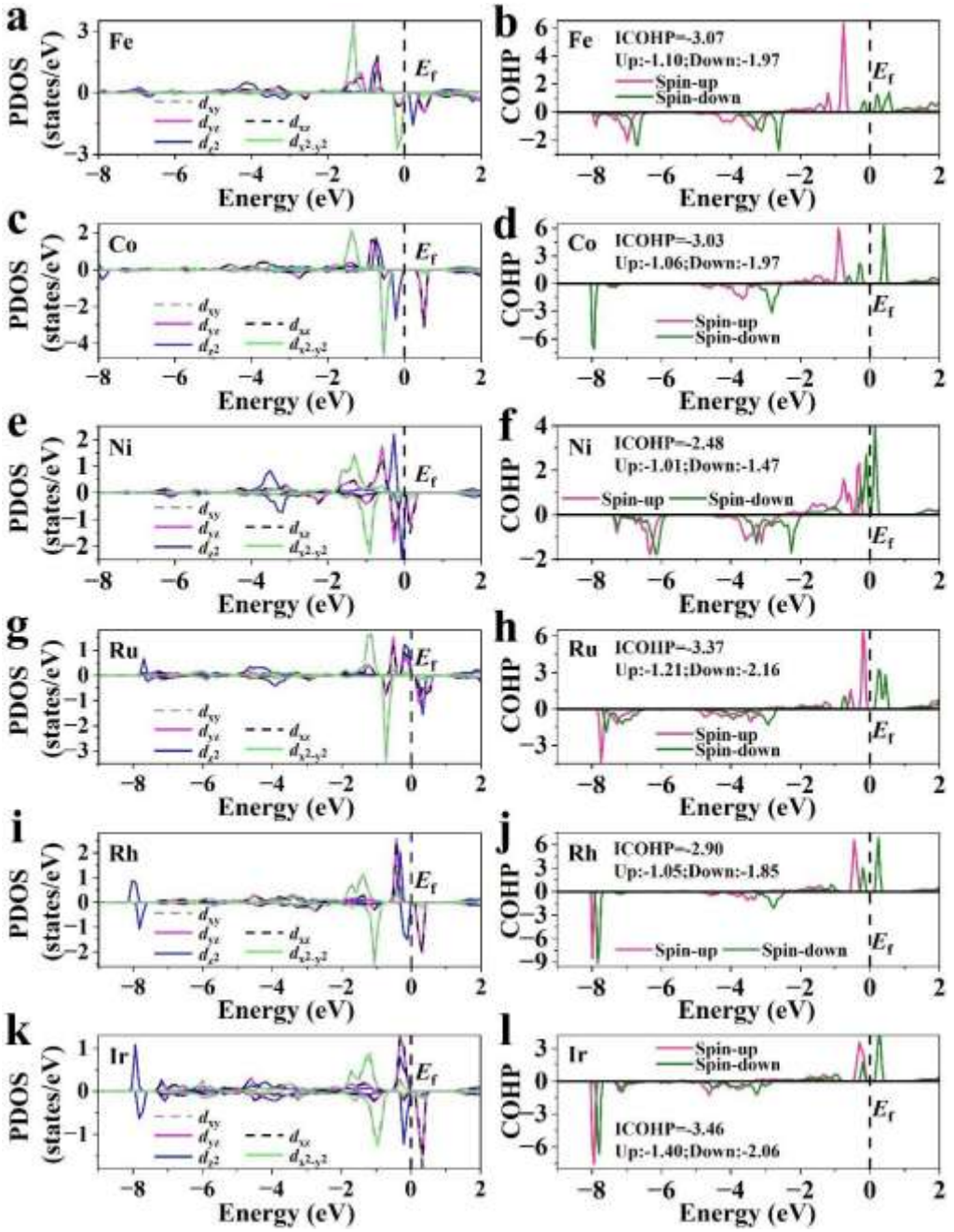

Fig. S20 Projected density of states and crystal orbital Hamilton population of TM@WS_2 systems upon *OH adsorption: (a, b) Fe, (c, d) Co, (e, f) Ni, (g, h) Ru, (i, j) Rh, and (k, l) Ir.

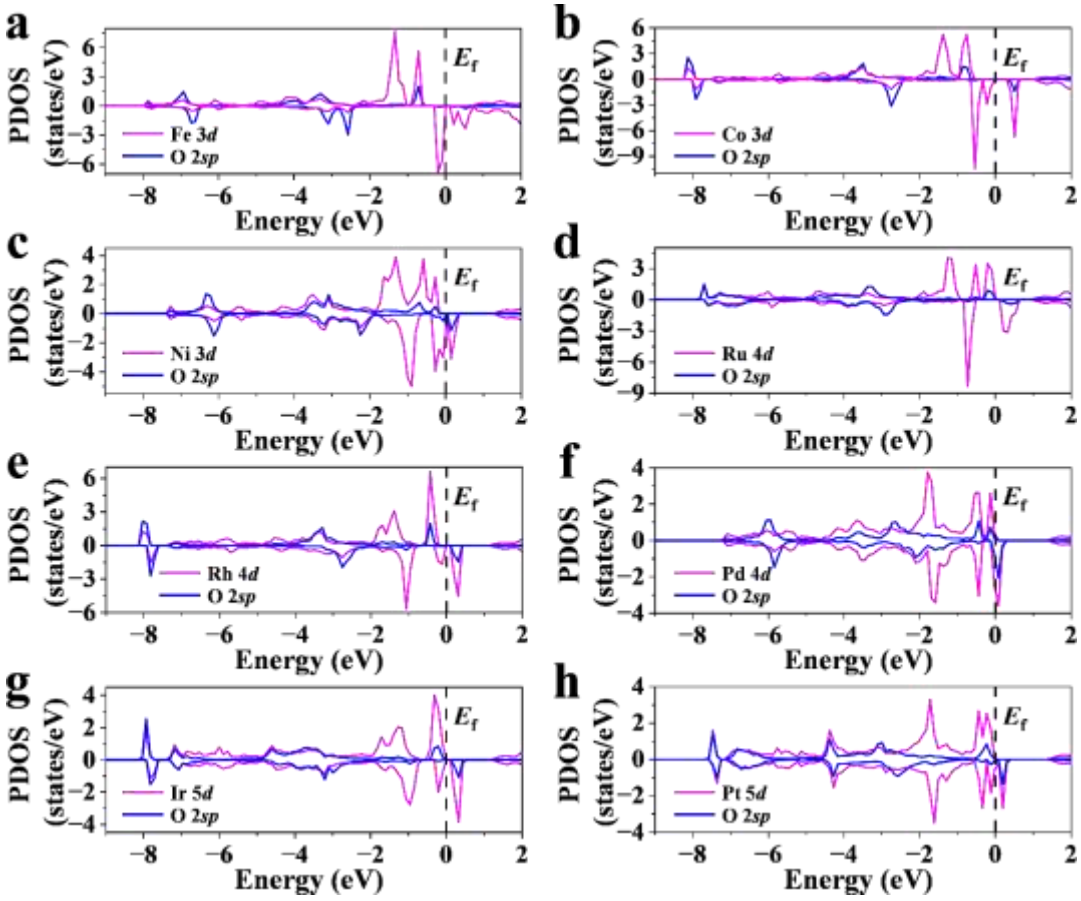

Fig. S21 Projected density of states (PDOS) of the *d* orbitals of TM atoms and the O 2*p* orbitals of the TM@WS_2 with adsorbed OH. Panels correspond to (a) Fe@WS_2, (b) Co@WS_2, (c) Ni@WS_2, (d) Ru@WS_2 and (e) Rh@WS_2, (f) Pd@WS_2, (g) Ir@WS_2, and (h) Pt@WS_2, respectively.

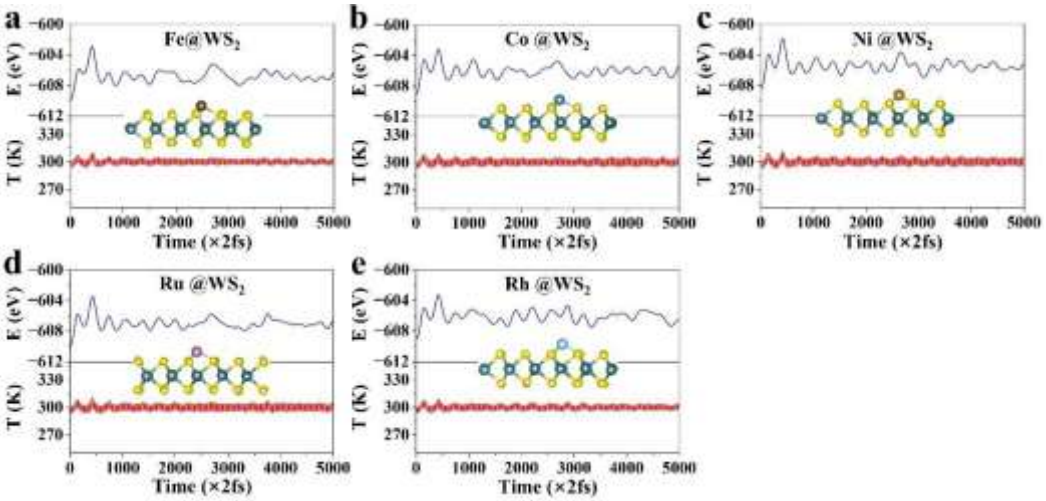

Fig. S22 Ab initio molecular dynamics (AIMD) simulations at 600 K for (a) Fe@WS_2, (b) Co@WS_2, (c) Ni@WS_2, (d) Ru@WS_2, and (e) Rh@WS_2, respectively.

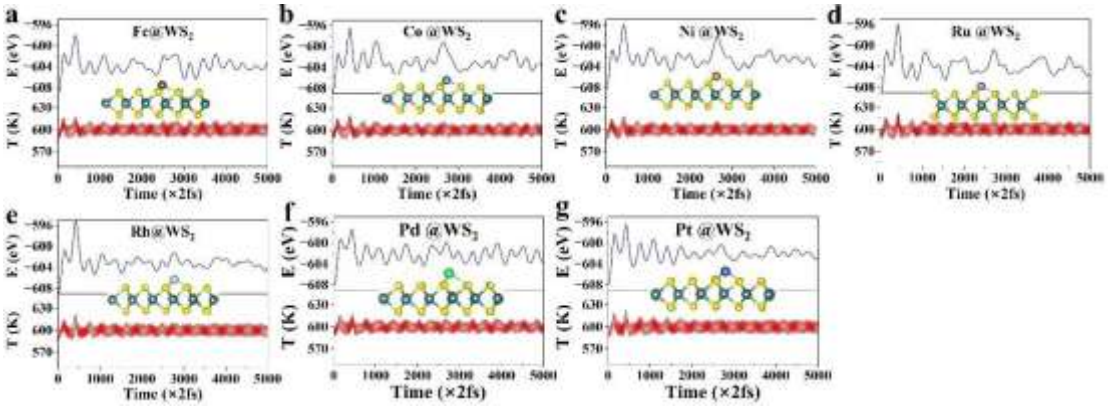

Fig. S23 Ab initio molecular dynamics (AIMD) simulations at 600 K for (a) Fe@WS_2, (b) Co@WS_2, (c) Ni@WS_2, (d) Ru@WS_2, (e) Rh@WS_2, (f) Pd@WS_2, (g) Pt@WS_2, respectively, respectively.

References

1. Nørskov, J. K.; Bligaard, T.; Logadottir, A.; Kitchin, J.; Chen, J. G.; Pandelov, S.; Stimming, U., Trends in the Exchange Current for Hydrogen Evolution, *J. Electrochem. Soc.*, **2005**, *152(3)*, J23.
2. He, T.; Gao, G.; Kou, L.; Will, G.; Du, A., Endohedral Metallofullerenes ($M@C_{60}$) as Efficient Catalysts for Highly Active Hydrogen Evolution Reaction, *J. Catal.*, **2017**, *354(*231-235.
3. Zhao, Y.; Zhang, J.; Ma, F.; Wu, H.; Meng, W.; Liu, Y.; Jiao, Y.; Du, A., Computational Exploration of Two-Dimensional Vacancy-Free Boridene Sheet and Its Derivatives: High Stabilities and the Promise for Hydrogen Evolution Reaction, *Microstructures*, **2024**, *4(3)*, 2024032.
4. Tian, X.; Zhao, P.; Sheng, W., Hydrogen Evolution and Oxidation: Mechanistic Studies and Material Advances, *Adv. Mater.*, **2019**, *31(31)*, 1808066.
5. Yang, X.; Lin, L.; Guo, X.; Zhang, S., Design of Multifunctional Electrocatalysts for ORR/OER/HER/HOR: Janus Makes Difference, *Small*, **2024**, *20(40)*, 2404000.
6. Gao, G.; O'Mullane, A. P.; Du, A., 2D Mxenes: A New Family of Promising Catalysts for the Hydrogen Evolution Reaction, *ACS Catal.*, **2017**, *7(1)*, 494-500.
7. Gao, G.; Jiao, Y.; Ma, F.; Jiao, Y.; Waclawik, E.; Du, A., Charge Mediated Semiconducting-to-Metallic Phase Transition in Molybdenum Disulfide Monolayer and Hydrogen Evolution Reaction in New 1T′ Phase, *J. Phys. Chem. C*, **2015**, *119(23)*, 13124-13128.
8. Tang, C.; Chen, L.; Li, H.; Li, L.; Jiao, Y.; Zheng, Y.; Xu, H.; Davey, K.; Qiao, S.-Z., Tailoring Acidic Oxygen Reduction Selectivity on Single-Atom Catalysts Via Modification of First and Second Coordination Spheres, *J. Am. Chem. Soc.*, **2021**, *143(20)*, 7819-7827.
9. Koh, S. W., et al., Two-Dimensional Palladium Diselenide for the Oxygen Reduction Reaction, *Mater. Chem. Front.*, **2021**, *5(13)*, 4970-4980.
10. Zheng, X.; Cao, X.; Sun, Z.; Zeng, K.; Yan, J.; Strasser, P.; Chen, X.; Sun, S.; Yang, R., Indiscrete Metal/Metal-N-C Synergic Active Sites for Efficient and Durable Oxygen Electrocatalysis toward Advanced Zn-Air Batteries, *Appl. Catal. B Environ.*, **2020**, *272(*118967.
11. Xie, L., et al., Edge-Doped Substituents as an Emerging Atomic-Level Strategy for Enhancing $M–N_4–C$ Single-Atom Catalysts in Electrocatalysis of the ORR, OER, and HER, *Nanoscale Horiz.*, **2025**, *10(2)*, 322-335.
12. Wang, Y.; Wang, M.; Lu, Z.; Ma, D.; Jia, Y., Enabling Multifunctional Electrocatalysts by Modifying the Basal Plane of Unifunctional 1T′-MoS_2 with Anchored Transition Metal Single Atoms, *Nanoscale*, **2021**, *13(31)*, 13390-13400.
13. Guo, X.; Gu, J.; Lin, S.; Zhang, S.; Chen, Z.; Huang, S., Tackling the Activity and Selectivity Challenges of Electrocatalysts toward the Nitrogen Reduction Reaction Via Atomically Dispersed Biatom Catalysts, *J. Am. Chem. Soc.*, **2020**, *142(12)*, 5709-5721.